Improve Accuracy of Fingerprinting Localization with Temporal Correlation of the RSS

Xiaohua Tian, *Member, IEEE*, Mei Wang, Wenxin Li, Binyao Jiang, Dong Xu, Xinbing Wang, *Senior Member, IEEE*, and Jun Xu

Abstract—Recent study presents a fundamental limit of the RSS fingerprinting based indoor localization. In this paper, we theoretically show that the temporal correlation of the RSS can further improve accuracy of the fingerprinting localization. In particular, we construct a theoretical framework to evaluate how the temporal correlation of the RSS can influence reliability of location estimation, which is based on a newly proposed radio propagation model considering the time-varying property of signals from Wi-Fi APs. The framework is then applied to analyze localization in the one-dimensional physical space, which reveals the fundamental reason why localization performance can be improved by leveraging temporal correlation of the RSS. We extend our analysis to high-dimensional scenarios and mathematically depict the boundaries in the RSS sample space, which distinguish one physical location from another. Moreover, we develop an algorithm to utilize temporal correlation of the RSS to improve the location estimation accuracy, where the process for choosing key design parameters are provided through experiments. Experiment results show that the localization reliability and accuracy can be improved by up to 13 and 30 percent with appropriate leveraging the RSS temporal correlation information.

Index Terms—Fingerpringting, localization, temporal correlation

1 Introduction

Indoor localization based on RSS fingerprinting approach has been attracting many research efforts in the past decades, where the basic idea is to first construct RSS fingerprints database during the training phase, and then perform location estimation by matching the user's reported fingerprints in the database during the localization phase [1]. Indoor localization systems based on the approach have been developed with different flavors. Embedded sensors of mobile devices are exploited to improve accuracy of the location estimation [2], [3], crowdsourcing paradigm is used to reduce the cost of site survey in the training phase [4], and machine learning algorithms are leveraged to shorten the delay of localization process [5], [6], [7].

The spring-up of RSS fingerprinting based indoor localization systems promotes efforts to study performance bounds of such systems both empirically and theoretically. Empirical studies evaluate performance of localization systems with comprehensive experiments. Liu et al. present their experimental results showing that the location estimation error could be over 6 m [2]. Chandrasekaran et al. provide empirical quantification of accuracy limits of RSS localization, which is based on extensive experimental results conducted over a uniform testbed [8]. Such results could be helpful references for system implementation but hardly provide insight into the RSS fingerprinting approach. Some theoretical studies about localization performance bound are based on Cramér-Rao Bound (CRB) analysis [9], [10], [11]; the framework is based on the Log-Distance Path Loss (LDPL) radio propagation model [1], [8], which however has been proved inaccurate in the indoor localization scenarios [12].

Recently, Wen et al. present a theoretical investigation on RSS fingerprinting based indoor localization, which reveals fundamental limits of the localization methodology [13]. Specifically, the work derives a close-form expression for calculating the probability that a user can be correctly localized in a region of certain size, which is termed as localization reliability. The basic idea of the derivation is to build a probability space induced from RSS samples obtained from the training stage. The location determination process can be regarded as a mapping from the sample space to the physical space; therefore, the probability a user can be correctly localized in a certain region is equal to the probability that certain outcomes of RSS measurements appear, so that the localization system can determine the user's location to be in the region. As highly accurate indoor localization is essential to enable many location based services, a natural question to ask is: can we further improve the performance of the localization scheme fundamentally?

In this paper, we show that the temporal correlation of the RSS can improve accuracy of RSS fingerprinting based indoor localization. We first construct a theoretical framework to

- *X. Tian is with the School of Electronic Information and Electrical Engineering, Shanghai Jiao Tong University, Shanghai 200240, China, and the State Key Laboratory of Integrated Services Networks, Xidian University, Xian Shi 710126, China. E-mail: xtian@sjtu.edu.cn.*
- *M. Wang, W. Li, B. Jiang, D. Xu, and X. Wang are with the School of Electronic Information and Electrical Engineering, Shanghai Jiao Tong University, Shanghai 200240, China. E-mail: {mary1994, 469634196, emberspirit, whathexd, xwang8}@sjtu.edu.cn.*
- *J. Xu is with the School of Computer Science, Georgia Institute of Technology, Atlanta, GA 30332. E-mail: jx@cc.gatech.edu.*

Manuscript received 13 May 2016; revised 29 Dec. 2016; accepted 8 May 2017. Date of publication 12 May 2017; date of current version 1 Dec. 2017. (Corresponding author: Xiaohua Tian.)
For information on obtaining reprints of this article, please send e-mail to: reprints@ieee.org, and reference the Digital Object Identifier below.
Digital Object Identifier no. 10.1109/TMC.2017.2703892

analyze how the temporal correlation of the RSS can influence the accuracy of location estimation, which is based on a newly proposed radio propagation model considering the time-varying property of signals from a given Wi-Fi AP. Based on such a model, we build a new sample space from the training phase, where each outcome in the space is extended with a new temporal dimension (Section 3).

We then apply the theoretical framework to analyze the localization process in the one-dimensional physical space, which reveals the fundamental reason why performance of localization can be improved by leveraging temporal correlation of the RSS. An interesting finding is that: the boundary in the sample space used to distinguish one physical location from another, in fact should be one edge of hyperbola, instead of a line as believed in most of the work in the literature; moreover, we find that the curvature of the hyperbola is related to the correlation of the RSS in the sample space. (Section 4) Such finding can fundamentally improve accuracy of location estimation of the RSS fingerprinting based system.

We extend our analysis to high-dimensional scenarios, where high temporal and sample space dimensions, and two-dimensional physical space are taken into account. The major challenge for the high-dimensional case is to deal with the complicated relationship between the location in the physical space and the corresponding temporal correlation of the RSS in the sample space. We propose to approximate the covariance matrix of the RSS in a location with a simplified matrix, which enables finding the boundaries that are asymptotically equivalent to the original ones. We then mathematically depict the boundaries in the sample space that distinguish the one physical space from another in the high temporal, sample space and physical space dimensions (Section 5).

Further, we develop an algorithm to improve performance of the location estimation utilizing temporal correlation of the RSS. The basic idea is using the mean of the RSS to find a list of candidate locations the user could be currently at, and then leveraging the temporal correlation to choose the best estimaton on the list. We conduct experiments to show the feasibility of the algorithm and choose key design parameters for the algorithm (Section 6). We also apply the algorithm in the practical location estimation process, and the results show that the localization reliability and accuracy can be improved by up to 13 and 30 percent respectively with appropriate leveraging the RSS temporal correlation information (Section 7). Due to the limitation of the space, we put some detailed theoretical derivation and experimental results in our technical report [15].

2 Related Work

2.1 Fundamental Limits of RSS Fingerprinting Approach

Wen et al. present a theoretical investigation on RSS fingerprinting based indoor localization, which reveals fundamental limits of the localization methodology [13]. Specifically, if a user's real location is at Q, a close-form expression of the probability R that the user can be localized in the δ neighborhood of Q could be derived, where δ and R are used to benchmark localization accuracy and reliability, respectively.

With the RSS fingerprinting based localization approach, RSS fingerprints obtained from the training stage form a sample space, based on which a user's location in the physical space can be estimated. The location determination process can be regarded as a mapping from the sample space to the physical space. If outcomes of RSS measurements fall into the event region $\mathbb{E}$, then the localization system can correctly determine the location of the user to be in the δ neighborhood of Q; therefore, the localization reliability is equal to the probability that outcomes of RSS measurements fall into the event region $\mathbb{E}$. By constructing a general radio propagation model based on field observations of real localization systems, probabilities for outcomes of RSS measurements in a location can be presented, which turns out to be following Gaussian distribution. Consequently, calculating the localization reliability is to first find the event region $\mathbb{E}$ in the RSS sample space, and then perform integration over the region $\mathbb{E}$ for an Gaussian probability density function (PDF).

Although utilizing a general radio propagation model, the study in [13] is distinguishable from the model based localization because the radio propagation model is not used to derive geometric relationships between signal transmitters and receivers, such as distance, time of arrival (ToA), time difference of arrival (TDoA) or angle of arrival (AoA) [1]. That is why the radio propagation model used in [13] only assumes that the mean of RSS readings varies with respect to locations but does not specify how the mean will vary. This is in contrast to the LDPL model used in the model based localization and CRB analysis [9], [10], [11], [42], where the mean varies with respect to locations logarithmically. Moreover, interesting findings about the shape of the event region $\mathbb{E}$ are presented in [13], where skillful mathematical techniques are demonstrated. We note that efforts have been made to estimate the user's location with channel state information (CSI) [31], [32], [33]; however, this vein of work is highly dependent on the device that provides the CSI [34]. In practice, the CSI is still not provided by most if not all of manufacturers to the best of our knowledge.

The localization techniques mentioned above are basically utilizing networking infrastructures that are dedicated to communication instead of localization. A series work has been done to study a new paradigm of wireless networks considering not only communication but also contextual information collection and navigation, which is known as network localization and navigation [39]. Under such a paradigm, some interesting issues emerge such as the joint optimization of localization and power allocation [40]. Wymeersch et al. present a systematical study of cooperative localization algorithms and apply them to the ultrawide bandwidth (UWB) wireless network [41].

Our study constructs a new radio propagation model considering the temporal correlation of the RSS, which is not taken into account in [13]. The later discussions are to reveal that the boundary distinguishing one location from another in the sample space is different from that shown in [13], and the new boundary provides more accurate location estimations. Compared with the pure theoretical analysis presented in [13], we present experimental results to validate our theoretical analysis.

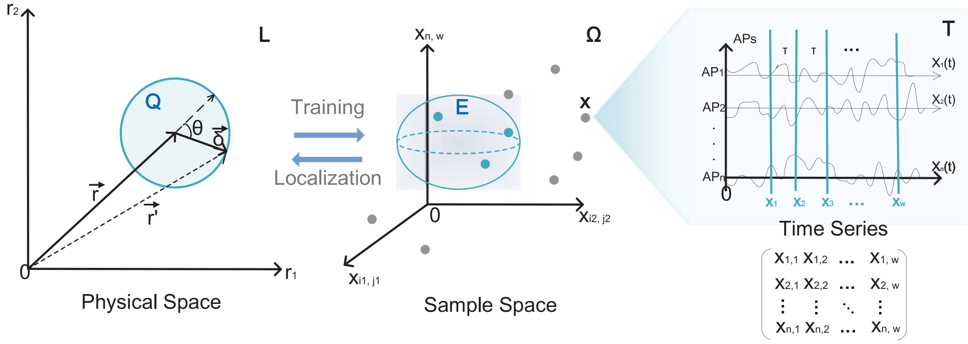

Fig. 1. Theoretical localization model.

2.2 Temporal Information of RSS Utilized for Localization

Kaemarungsi et al. study properties of the RSS for fingerprinting based localization using Wi-Fi [35]. Comprehensive experiment results reveal two important features of the RSS: First, the mean and variance of the RSS in one location basically remain the same over time; second, the auto-covariance function of the RSS in one location has the same shape for separate time-series. Based on such two observations, our work in this paper models the RSS observed in one location as a stationary process. Fang et al. propose a localization approach based on the dynamic system and machine learning technique [6]. Such an approach estimates the user's location by the state consisting of RSSes observed in different times and locations. However, the simple combination of spatial and temporal information does not reveal the essence how the temporal information can be utilized for localization, where the RSS observed in different times can be considered as multiple measurements of fingerprints.

Most of the current studies for utilizing temporal information of the RSS for localization are in a machine-learning based manner [5], [7], where the theoretical explanation about how the temporal information can influence the performance of the localization process is still unavailable. In this paper, we initiate the theoretical study on this issue.

3 Theoretical Model of Location Estimation

Consider an indoor space, which can be modeled as one or two dimensional Cartesian space denoted by $L \subset \mathbb{R}$ or $L \subset \mathbb{R}^2$, respectively. Examples of one dimensional model include hallway and corridor. A user's location in the physical space S can be denoted by $\vec{r} = r_1$ or $\vec{r} = (r_1, r_2)$ with corresponding dimensions. Based on the localization database constructed in the training phase, a sample space of fingerprints can be induced, which is denoted by Ω^n and n is the number of access points (APs) can be sensed in the physical space. In the training phase, the site surveyor collects fingerprints of APs in a one-by-one manner at a given location. For an AP, the surveyor samples the observed RSS at certain frequency. Consequently, if there are n APs and each AP is sampled w times, then a point $\mathbf{x}$ in the RSS sample space is as shown in the right part of Fig. 1, where $x_{i,j}$ means the RSS observed with respect to AP_i at jth time point. We say this is an n-dimensional sample space and the temporal dimension of sampling is w.

As the radio propagation in the indoor environment is influenced by many factors such as path loss, shadowing, fading and multipath effect, the signal can be observed in a location is usually modeled as a random process, which can be denoted by

$$X(\vec{r}, \vec{t}) = S(\vec{r}) + \sigma Y(\vec{r}, \vec{t}), \tag{1}$$

where $\vec{r}$ is the location of the observation and $\vec{t}$ represents the vector of time points at which RSSes are observed. $S(\vec{r})$ is the trend model of the signal with respect to position $\vec{r}$ in the perspective of stochastic processes, σ is the amplitude of the randomness, and $Y(\vec{r}, \vec{t})$ is the joint Gaussian distribution of temporal randomness at location $\vec{r}$.

This radio propagation model is generalized from the LDPL radio propagation model, and enhanced with the temporal domain characteristic. If a time point t is given, the model degenerated into the radio propagation model in [13], where the RSS can be modeled as a Gaussian random variable with fading and multipath effects integrated into a mean function such as $S(\vec{r})$. Such modeling is widely adopted in the literature on indoor localization in the past decade [1], [12], [17], [18], [19], [20], [21]. With the temporal dimension considered in this paper, the RSS is modeled as a Gaussian stochastic process, which is also verified by a number of work in the literature [22], [23], [24], where and the temporal correlation by the shadowing effect incurred by the fixed building structure is modeled with $\sigma Y(\vec{r}, \vec{t})$.

According to extensive experimental results and theoretical analysis [36], [37], [38], the mean and variance of the RSS in one location basically remain the same over time and the auto-covariance function of the RSS in one location has the same shape for separate time-series, such a random process can be stationary and ergodic, with

$$S(\vec{r'}) \approx S(\vec{r}) + \bigtriangledown S(\vec{r})(\vec{r'} - \vec{r}). \tag{2}$$

In the localization phase, a user reports observed RSSes to the localization server, which then estimates the corresponding location by matching the reported fingerprints in the fingerprints database. Such a process can be modeled as a mapping from the sample space to the physical space

$$M : \Omega^n \to L, \quad \vec{r'} = M(\mathbf{X}(\vec{r}, \vec{t})), \tag{3}$$

where $\vec{r'}$ is the estimated location of the user. This process is illustrated in Fig. 1. The user's actual location is at $\vec{r}$ and the estimated location is at $\vec{r'}$, which incurs the localization error denoted by $\vec{\delta}$.

Due to estimation errors, the result of the localization is that the user's location is estimated to be in the δ

neighborhood of $\vec{r}$, which is denoted by Q. To reduce the error of localization is equivalent to mitigating the norm of $\vec{\delta}$. Since the basis of the estimation is the reported fingerprint by the user, the ideal case is that the user's submitted fingerprints happen to make the system believe that the location of the user is in Q. We use $\mathbb{E}$ to denote such a region in the sample space, so that the user's location can be estimated to be in Q as long as the reported RSSes fall in $\mathbb{E}$.

The probability that the reported RSS fingerprints can fall into the region of $\mathbb{E}$ depends on the model of radio signal propagation, which in fact fundamentally determines the performance of the RSS fingerprinting based approach. The model proposed in [13] considers the observed RSS at one location as a random variable, where temporal correlation of the signal is not taken into account. According to the site survey practice, it is more practical to model the signal as a random process as in this paper, where the temporal correlation can be leveraged.

Our investigation in this paper focuses on the influence of temporal correlation of the RSS on performance of localization. We are to show that such a seemingly slight change in the radio signal propagation modeling could help reveal interesting findings of the RSS fingerprinting based approach, which have never been presented; the corresponding difficulties in mathematical analysis is definitely non-trivial. It is worth mentioning that the body-shadowing effect incurred by people's mobility also could influence the radio propagation in the indoor space [27], which is actually an important research field with many efforts dedicated [28], [29], [30]. The body-shadowing effect will be considered in our future work, since taking account of too many factors will make the mathematical analysis untractable and hinders revealing the insight.

4 Analysis of 2-D Temporal Correlation for 1-D Localization

This section examines a concrete scenario of localization, where both the physical space and the sample space are one dimensional and the temporal dimension of sampling is two. The purpose of the examination is to find how likely the user can be localized in Q with given δ. It is easier to reveal essence of the fingerprinting approach by analyzing a simple case, where the results could be inspiring for analyzing more complicated scenarios.

4.1 Finding Region $\mathbb{E}$

Let us first find out what kind of RSSes can be observed at the location $\vec{r}$. The one-dimensional physical space can be regarded as an one-dimensional horizontal axis, where the origin of the axis is the location of the AP, and the location of each point can be identified by a scalar r. Based on the radio signal propagation model, the probability density function of RSS readings can be observed follows the Multivariate Guassian Distribution

$$f_r(x_1,x_2)=\frac{1}{2\pi\sigma^2\sqrt{1-\rho^2}}e^{-\frac{1}{2}\Delta^2}, \tag{4}$$

where x_1, x_2 are variables representing the RSSes at time points t_1 and t_2 separated by a duration of τ as shown in

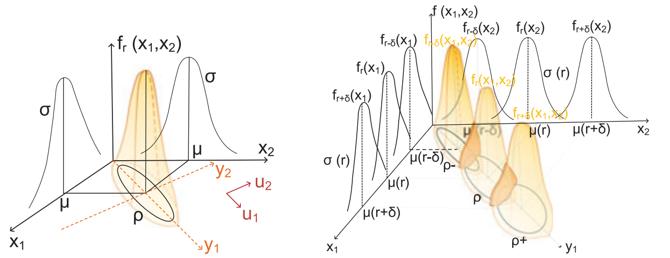

(a) Joint Gaussian PDF of $RSS(t)$ and $RSS(t+\tau)$ at position $\mathbf{r}$.

(b) Joint Gaussian PDFs at Different Locations.

Fig. 2. Joint Gaussian PDF.

Fig. 2a. Since the random process representing the signal is stationary, the following analysis is oblivious to the specific value of t_1 and t_2 as long as they are separated by τ. Symbols μ and σ are the mean and standard variance of the RSS joint distribution at position $\vec{r}$, respectively; ρ is the autocorrelation coefficient of $f_r(x_1,x_2)$. The Mahalanobis distance is denoted as Δ, where

$$\Delta^2=\frac{1}{\sigma^2(1-\rho^2)}[(x_1-\mu)^2+(x_2-\mu)^2-2\rho(x_1-\mu)(x_2-\mu)]. \tag{5}$$

Since x_1 and x_2 are both observed at r, the corresponding marginal distributions with respect to x_1 and x_2 are the same, according to our signal propagation model; the corresponding means and standard variances of the two marginal distributions are the same as well. This also complies with the conclusion in [13]. Consequently, the covariance matrix of $f_r(x_1,x_2)$ is real, positive and symmetric, where

$$\Sigma=\sigma^2\begin{bmatrix}1 & \rho\\ \rho & 1\end{bmatrix}. \tag{6}$$

With the same reason, the major axis of the elliptical surface representing $f_r(x_1,x_2)$ should be the angular bisector of the Cartesian coordinates with slope 1.

In order to facilitate our analysis, we put the image of $f_r(x_1,x_2)$ in a new coordinates system with axes y_1 and y_2. We let the major axis of the elliptical surface align to y_1 and the origin of the new coordinates system be $(\mu(r),\mu(r))$ in the old system. Then the PDF in the new system is

$$f_r(y_1,y_2)=\frac{1}{2\pi\sigma^2\sqrt{\lambda_1\lambda_2}}e^{-\frac{1}{2\sigma^2}(\frac{y_1^2}{\lambda_1}+\frac{y_2^2}{\lambda_2})}, \tag{7}$$

where

$$\lambda_1=\frac{\sqrt{2}(1+\rho)}{2},\lambda_2=\frac{\sqrt{2}(1-\rho)}{2}. \tag{8}$$

We now start to find the region $\mathbb{E}$ in this scenario. Refer to Fig. 2b, the value of $f_r(y_1,y_2)$ in fact means how likely the user can observe $[y_1,y_2]$ at location r. If the reported RSSes $[y_1,y_2]$ indicate that the user's location is in a small neighborhood of r, then $f_r(y_1,y_2)$ should be higher than $f_{r\pm\delta}(y_1,y_2)$, where $r\pm\delta$ are boundaries of r's neighborhood in the physical space. That is, if the user is localized in the

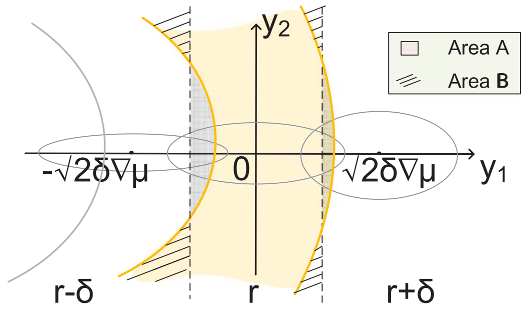

Fig. 3. Graphical illustration of region $\mathbb{E}$.

neighborhood of r, the corresponding submitted fingerprints should have fallen into the region

$$\mathbb{E} = \{\mathbf{x} | f_r(\mathbf{y}|\mu(r), \Sigma(r)) \geq f_{r\pm\delta}(\mathbf{y}|\mu(r\pm\delta), \Sigma(r\pm\delta))\}. \tag{9}$$

The profile of $\mathbb{E}$ is sketched in Fig. 2b, which is the space between the two regions in dark color. The two dark-colored regions themselves represent boundaries of intersected neighboring dome-like bodies. Observe marginal PDFs with respect to x_2 for the three locations $r-\delta$, r and $r+\delta$, which are presented by three Gaussian PDF curves on the $x_2 - f(x_1, x_2)$ plane with means $\mu(r-\delta)$, $\mu(r)$ and $\mu(r+\delta)$, respectively. It is worth mentioning that shapes of the three curves are the same, which is determined by the variance of Gaussian noise. This is because Gaussian noise at different locations in a small neighborhood of the physical space are presenting indistinguishable randomness, which have been acknowledged by extensive studies [13], [35]. Due to symmetry of the dome-like bodies, the same thing happens to the marginal PDFs with respect to x_1.

If the temporal correlation of the RSS is not considered, fingerprints can be observed at different time points with respect to the same AP are independent at each location; therefore, the randomness of the RSS can only be characterized in a 2-D curve of the marginal PDF as shown in Fig. 2b. Using such randomness to evaluate the performance limit of fingerprinting localization is the basic idea in [13].

Our work in this paper characterizes randomness of the RSS with the dome-like bodies as shown in Fig. 2b, where the temporal correlation of the signal is taken into account. We can see that our model presents a more accurate description of the randomness of the RSS, where a straightforward observation is the increase of a dimension. Such a model of the RSS provides more distinguishable characteristics of a location compared with that in [13], thus provides criteria of finer-granularity for localization. This is the fundamental reason why the accuracy performance bound of localization derived in [13] can be further improved if the RSS temporal correlation is taken into account.

4.2 Analysis on Region $\mathbb{E}$

Since the location estimation is performed based on fingerprints reported by the user, studying properties of $\mathbb{E}$ can help reveal how the system estimates the user's location. Intuitively, if we project the image in Fig. 2b onto the $y_1 - y_2$ coordinates system, the resulted image should be that as shown in Fig. 3. The region in yellow should be the projection of the space $\mathbb{E}$, and the two curves in yellow should be boundaries of the region. Consequently, if a user's reported fingerprints fall into the area left to $\mathbb{E}$, the user is more likely at the location $r-\delta$; if the reported fingerprints fall into the area right to $\mathbb{E}$, the user is more likely at the location $r+\delta$. We are to reveal that the boundaries of $\mathbb{E}$ are in the shape of hyperbolic curve with interesting properties, and then reveal challenges for accurately describing the region $\mathbb{E}$ with corresponding analysis provisioned.

4.2.1 Boundaries of Region $\mathbb{E}$

Substituting Eq. (7) into Eq. (9), we obtain the following inequality:

$$\frac{1}{\sqrt{\lambda_1\lambda_2}} e^{-\frac{1}{2\sigma^2}\left(\frac{y_1^2}{\lambda_1}+\frac{y_2^2}{\lambda_2}\right)} \geq \frac{1}{\sqrt{\lambda_1^{\pm}\lambda_2^{\pm}}} e^{-\frac{1}{2\sigma^2}\left(\frac{(y_1\pm\sqrt{2}\delta\nabla\mu)^2}{\lambda_1^{\pm}}+\frac{y_2^2}{\lambda_2^{\pm}}\right)}, \tag{10}$$

where λ_1, λ_2 are scaling factors of ellipse axes for Gaussian PDF at position r, and $\lambda_1^{\pm}, \lambda_2^{\pm}$ are scaling factors at adjacent positions $r\pm\delta$. Specifically,

$$\lambda_1^{\pm} = \frac{\sqrt{2}(1+\rho^{\pm})}{2}, \lambda_2^{\pm} = \frac{\sqrt{2}(1-\rho^{\pm})}{2}. \tag{11}$$

Symbols $\rho, \rho^{\pm}$ are the autocorrelation coefficients for the Gaussian distribution at r and $r\pm\delta$, respectively. After simplification, they are equivalent to

$$\begin{cases} \left(\frac{y_1^2}{\lambda_1}+\frac{y_2^2}{\lambda_2}\right) - \left(\frac{(y_1+\sqrt{2}\delta\nabla\mu)^2}{\lambda_1^{+}}+\frac{y_2^2}{\lambda_2^{+}}\right) \leq \ln\frac{\lambda_1\lambda_2}{\lambda_1^{+}\lambda_2^{+}}; \\ \left(\frac{y_1^2}{\lambda_1}+\frac{y_2^2}{\lambda_2}\right) - \left(\frac{(y_1-\sqrt{2}\delta\nabla\mu)^2}{\lambda_1^{-}}+\frac{y_2^2}{\lambda_2^{-}}\right) \leq \ln\frac{\lambda_1\lambda_2}{\lambda_1^{-}\lambda_2^{-}}, \end{cases} \tag{12}$$

which is the specific expression of $\mathbb{E}$ in the sample space. The boundaries of $\mathbb{E}$ can be obtained when the equality holds.

In order to better understand properties of the boundaries, we transform the expressions in inequalities (12) into a general form

$$Ay_1^2 + By_1y_2 + Cy_2^2 + Dy_1 + Ey_2 + F = 0, \tag{13}$$

where the discriminant Δ equals to

$$\Delta = B^2 - 4AC, \tag{14}$$

and $A = \frac{1}{\lambda_1} - \frac{1}{\lambda_1^{\pm}}$, $C = \frac{1}{\lambda_2} - \frac{1}{\lambda_2^{\pm}}$. Since $B = 0$, $AC < 0$, then $\Delta > 0$. This means that the two boundaries of $\mathbb{E}$ are in the shape of the hyperbolic curve, where the two foci are on axis y_1.

Note that if $A = C$ and $B = 0$, both of the boundaries are straight lines in parallel. $A = C$ and $B = 0$ also mean that $\lambda_1 = \lambda_2$, $\lambda_1^{\pm} = \lambda_2^{\pm}$, which is to say that measurements with respect to the same AP at different time points are totally independent. This is a degenerated scenario without considering temporal correlation as shown in [13]. The resulted straight-line boundaries are the same as corresponding boundaries of $\mathbb{E}$ in [13]. This is actually corroborating our current result about the shape of boundaries.

4.2.2 Accurate Description of $\mathbb{E}$

Although we have a basic idea about boundaries of $\mathbb{E}$, it is still non-trivial to theoretically prove that the region $\mathbb{E}$ is the

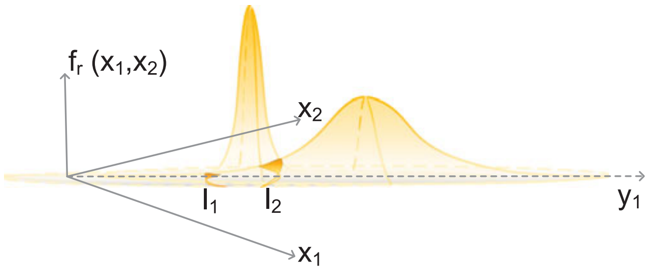

Fig. 4. Intersection of two Gaussian PDFs.

same as the intuition as shown in Fig. 3. Imagine the detailed scenario that two surfaces representing two joint Gaussian PDFs are intersecting with each other. There are actually two curves of intersection, as the two curves l_1 and l_2 illustrated in Fig. 4. This can be mathematically proved through simple derivation by constructing an equation between the two joint Gaussian PDFs.

It is slightly tricky to understand Figs. 2b and 4. Projections of those domes on planes x_1-$f(x_1, x_2)$ and x_2-$f(x_1, x_2)$ are the same in profile, because this is actually ignoring the temporal correlation of the RSS. Mathematically, the covariance matrix of $f_r(x_1, x_2)$ becomes variance σ^2 as the autocorrelation coefficient $\rho = 0$. However, those joint Gaussian PDFs factually have different autocorrelation coefficients denoted by ρ and $\rho^{\pm}$, as shown in Fig. 2b; therefore, if we project those domes on the plane y_1-$f(x_1, x_2)$, the resulted image is just that illustrated in Fig. 4.

In the perspective of engineering, the system considers that observing fingerprints around the l_1 is with very low probability if the user is at r, thus it is more meaningful to consider the boundary represented by l_2, in order to ensure an expected localization reliability as high as possible. It is worth mentioning that fingerprints such as those around l_1 indeed can be observed in practice. In this case, the system will estimate the location of the user is at r', where $f_{r'}(y1, y2)$ has a higher value, although the user is factually at r. Such errors can not be avoided in the fingerprinting based approach, since small probability events do happen.

We can see that the opening orientation of the boundaries illustrated in Fig. 2b is to the left. Refer to equalities (11), (12) and Fig. 3, if $\rho^- < \rho < \rho^+$, the physical meaning of the inequalities (12) is that: all points with the distance differences between $r - \delta$ to r and r to $r + \delta$ are less than a constant. The opening orientation is to the left, according to the definition of the hyperbola. If $\rho^- > \rho > \rho^+$, the physical meaning of the inequalities (12) is that: all points with the distance differences between r to $r - \delta$ and $r + \delta$ to r are less than a constant. The opening orientation is to the right. For convenience of presentation, we here abuse the coordinate in the physical space and use the coordinate to represent the corresponding RSS values in the y_1 axis.

This means that the opening orientation of boundaries are actually determined by the degree of temporal correlation of the RSS at different locations. Moreover, no matter the relationship among ρ and $\rho^{\pm}$, the inequalities of (12) show that $\mathbb{E}$ is in the middle of the two boundaries. As a matter of fact, if we specifically consider the real situation under study, it should be the case $\rho^- < \rho < \rho^+$. Recall our 1-D physical model, where the AP is located at the origin of an 1-D coordinate axis and $r - \delta$, r and $r + \delta$ are distance to the AP. The farther the location is from the AP, the stronger the temporal correlation of the observed RSS will be; consequently, the orientations of the two boundaries should be to the left as shown in Fig. 3.

4.3 Influence of Temporal Correlation on Accuracy of Localization

We can further verify our theory by examining the expected localization result given special fingerprints. The point $(-\sqrt{2}\delta\nabla\mu,\ 0)$ in Fig. 4 is special, which makes $f_{r-\delta}(-\sqrt{2}\delta\nabla\mu, 0)$ to achieve the maximum value. This means that if a user reports fingerprints $(-\sqrt{2}\delta\nabla\mu,\ 0)$, the system definitely should estimate the user's location to be at $r - \delta$. Substituting $(-\sqrt{2}\delta\nabla\mu,\ 0)$ into the first inequality of (12), A natural consequence is supposed to be that the point $(-\sqrt{2}\delta\nabla\mu,\ 0)$ is definitely to the left of the left boundary of $\mathbb{E}$. However, we are surprised to find that it is possible for the point $(-\sqrt{2}\delta\nabla\mu, 0)$ to be within the region $\mathbb{E}$. That is, the point $(-\sqrt{2}\delta\nabla\mu,\ 0)$ is to the right of the left boundary of $\mathbb{E}$. This can happen if we set δ to be very small and the difference between ρ^- and ρ to be very large. The grey curve shown in Fig. 4 is the resulted boundary if we choose special values of δ and ρ. This event can lead to errors of location estimation, because a user definitely should be localized at $r - \delta$ is in fact localized at r.

The root cause of the phenomenon is that the choice of δ and ρ in a theoretical perspective may not comply with the real situation. In the real world, the temporal correlation in a small neighborhood with respect to the same AP should be varying smoothly. Consequently, if δ is small, the difference between ρ^- and ρ is supposed to be insignificant.

We now compare localization results yielded by considering and ignoring the temporal correlation of the RSS. Recall the study in [13] ignores the temporal correlation of the RSS. The region $\mathbb{E}$ in this case is the region between the two dashed lines as shown in Fig. 4. Consider shadowed areas B covered with solid lines. If the user's reported fingerprints fall into such areas, it means that the user supposed to be localized at r is mistakenly localized at $r - \delta$, or the user supposed to be localized at $r + \delta$ is mistakenly localized at r. Similarly, consider the grey areas A. If the user's reported fingerprints fall into such areas, it means that the user supposed to be localized at $r - \delta$ is mistakenly localized at r, or the user supposed to be localized at r is mistakenly localized at $r + \delta$. That is, considering temporal correlation can improve the accuracy of location estimation by providing more accurate criteria for making judgement.

5 Asymptotic Equivalent Region of $\mathbb{E}$ in High-Dimensional Scenarios

We extend our analysis to scenarios of high-dimensional temporal correlation, sample space and physical space in our conference version [14]; however, it is difficult to obtain the exact information about the shape of $\mathbb{E}$ due to the high dimension and complicated interrelation between the physical space and sample space. In this section, we try to find a close-form description of $\mathbb{E}'$ that is asymptotically equivalent to $\mathbb{E}$, so that a quantified understanding of $\mathbb{E}$ could be provided.

5.1 Approximate Matrix

The covariance matrix of the RSS at location $\vec{r}$ is denoted by $\Sigma_m(\vec{r})$. For the correlation coefficients, it is reasonable that

$$\rho_i(\vec{r'}) \approx \rho_i(\vec{r}) + \nabla\rho_i(\vec{r})(\vec{r'} - \vec{r}), \tag{15}$$

because the correlation of the RSS is continuous, which has been verified in our experiments to be presented in [15]. Then we have

$$\Sigma_m(\vec{r'}) = \Sigma_m(\vec{r}) + \delta\cos\theta \begin{bmatrix} |\nabla\rho_0(\vec{r})| & |\nabla\rho_1(\vec{r})| & |\nabla\rho_2(\vec{r})| & \cdots & |\nabla\rho_{m-1}(\vec{r})| \\ |\nabla\rho_1(\vec{r})| & |\nabla\rho_0(\vec{r})| & |\nabla\rho_1(\vec{r})| & \ddots & |\nabla\rho_{m-2}(\vec{r})| \\ |\nabla\rho_2(\vec{r})| & |\nabla\rho_1(\vec{r})| & \ddots & \ddots & \vdots \\ \vdots & \ddots & \ddots & \ddots & |\nabla\rho_1(\vec{r})| \\ |\nabla\rho_{m-1}(\vec{r})| & \cdots & |\nabla\rho_2(\vec{r})| & |\nabla\rho_1(\vec{r})| & |\nabla\rho_0(\vec{r})| \end{bmatrix}. \tag{16}$$

We propose to use matrix $\Upsilon_m(\vec{r})$ to approximate $\Sigma_m(\vec{r})$, as shown in

$$\Upsilon_m(\vec{r'}) = \begin{bmatrix} \rho_0(\vec{r}) & \rho_1(\vec{r}) + \rho_{m-1}(\vec{r}) & \rho_2(\vec{r}) + \rho_{m-2}(\vec{r}) & \cdots & \rho_1(\vec{r}) + \rho_{m-1}(\vec{r}) \\ \rho_1(\vec{r}) + \rho_{m-1}(\vec{r}) & \rho_0(\vec{r}) & \rho_1(\vec{r}) + \rho_{m-1}(\vec{r}) & \ddots & \rho_2(\vec{r}) + \rho_{m-2}(\vec{r}) \\ \rho_2(\vec{r}) + \rho_{m-2}(\vec{r}) & \rho_1(\vec{r}) + \rho_{m-1}(\vec{r}) & \rho_0(\vec{r}) & \ddots & \vdots \\ \vdots & & \ddots & \ddots & \rho_1(\vec{r}) + \rho_{m-1}(\vec{r}) \\ \rho_1(\vec{r}) + \rho_{m-1}(\vec{r}) & \rho_2(\vec{r}) + \rho_{m-2}(\vec{r}) & \cdots & \rho_1(\vec{r}) + \rho_{m-1}(\vec{r}) & \rho_0(\vec{r}) \end{bmatrix}. \tag{17}$$

Suppose that the eigenvector of $\Upsilon_m(\vec{r})$ is $u = [\,u_1\; u_2 \cdots u_m]$, which satisfies that $\Upsilon_m(\vec{r})u = \tau(\vec{r})u$. It is easy to verify that vector $u(k) = [1, e^{i2\pi k/m}, e^{i2\pi 2k/m}, \ldots e^{i2\pi(m-1)k/m}]$ $(1 \leq k \leq m)$ satisfies the equations and the corresponding eigenvalue is

$$\tau_{m,k}(\vec{r}) = \rho_0(\vec{r}) + \sum_{j=1}^{m-1}(\rho_i(\vec{r}) + \rho_{m-i}(\vec{r}))e^{i2\pi jk/m}.$$

We note that $\tau_{m,k}(\vec{r})$ is a real number since the coefficients of complex conjugate pairs $e^{i2\pi jk/m}$ and $e^{i2\pi j(m-k)/m}$ are identical. For the eigenvalues at location $\vec{r'}$, we have

$$\begin{aligned}\tau_{m,k}(\vec{r'}) &= \rho_0(\vec{r'}) + \sum_{j=1}^{m-1}(\rho_i(\vec{r'}) + \rho_{m-i}(\vec{r'}))e^{i2\pi jk/m} \\ &= \tau_{m,k}(\vec{r}) + \delta\cos\theta\sum_{j=1}^{m-1}(|\nabla\rho_i(\vec{r})| + |\nabla\rho_{m-i}(\vec{r})|)e^{i2\pi kj/m}.\end{aligned}$$

To simplify the notations, we use $\Delta\tau_{m,k}$ to represent $\sum_{j=1}^{m-1}(|\nabla\rho_i(\vec{r})| + |\nabla\rho_{m-i}(\vec{r})|)e^{i2\pi kj/m}$, thus $\tau_{m,k}(\vec{r'}) = \tau_{m,k}(\vec{r})$ $+\delta\cos\theta\Delta\tau_{m,k}$.

We are to prove that using $\tau_{m,k}(\vec{r})$ to approximate eigenvalues of $\Sigma_m(\vec{r})$ could incur the approximation error converging to zero as m goes to infinity.

5.2 Asymptotical Equivalence Analysis

We take another form of region $\mathbb{E}$ as following to facilitate understanding:

$$\sum_{i=1}^{m}\frac{y_i{}^2}{\lambda_{m,i}(\vec{r})} - \left[\frac{(y_1 + \sqrt{2}\delta\nabla\cos\theta)^2}{\lambda_{m,1}(\vec{r'})} + \sum_{i=1}^{m}\frac{y_i{}^2}{\lambda_{m,i}(\vec{r'})}\right] \leq \ln\frac{|\Sigma(\vec{r})|}{|\Sigma(\vec{r'})|},$$

where $\theta \in [0, \pi]$. If we use eigenvalues of matrix $\Upsilon_m(\vec{r'})$ to replace $\lambda_i(\vec{r'})$, we could obtain the region $\mathbb{E}'$ characterized by the following equation:

$$\sum_{i=1}^{m}\frac{y_i{}^2}{\tau_{n,i}(\vec{r})} - \left[\frac{(y_1 + \sqrt{2}\delta\nabla\cos\theta)^2}{\tau_{m,1}(\vec{r'})} + \sum_{i=1}^{m}\frac{y_i{}^2}{\tau_{m,i}(\vec{r'})}\right] \leq \ln\frac{|\Upsilon_m(\vec{r})|}{|\Upsilon_m(\vec{r'})|}.$$

Lemma 1. $\lim_{m\to\infty}|\Upsilon_m(\vec{r}) - \Sigma(\vec{r})|^2 = 0$, *where* $|\cdot|^2$ *represents the Hilbert-Schmidt Norm.*

Proof.

$$\Upsilon_m(\vec{r}) - \Sigma(\vec{r}) = \begin{bmatrix} 0 & \rho_{m-1}(\vec{r}) & \rho_{m-2}(\vec{r}) & \cdots & \rho_1(\vec{r}) \\ \rho_{m-1}(\vec{r}) & 0 & \rho_{m-1}(\vec{r}) & \ddots & \rho_2(\vec{r}) \\ \rho_{m-2}(\vec{r}) & \rho_{m-1}(\vec{r}) & 0 & \ddots & \vdots \\ \vdots & & \ddots & \ddots & \rho_{m-1}(\vec{r}) \\ \rho_1(\vec{r}) & \rho_2(\vec{r}) & \cdots & \rho_{m-1}(\vec{r}) & 0 \end{bmatrix}.$$

With the definition of *Hilbert-Schmidt Norm*,

$$|\Sigma(\vec{r}) - \Upsilon_n(\vec{r})|^2 = 2\sum_{i=1}^{n-1}\tfrac{i}{n}\,\rho_i^2(\vec{r}),$$

we will show that

$$\lim_{m\to\infty}\sum_{i=1}^{m-1}\tfrac{i}{m}\,\rho_i^2(\vec{r}) = 0.$$

By applying *Abel Transformation* to the equation above, we obtain that

$$\sum_{i=1}^{m-1} \tfrac{i}{m}\, \rho_i^2(\vec{r}) = \frac{m-1}{m} A_{m-1} - \sum_{i=1}^{m-2} \frac{1}{m} A_i,$$

where $A_i = \sum_{j=1}^{i} \rho_j^2(\vec{r})$. Since the covariances are absolutely summable with $\sum_i \rho_i < \infty$, we use A to denote the supremum of $\sum \rho_j^2(\vec{r})$, i.e., $A = \sup \sum \rho_j{}^2(\vec{r})$. Consequently, we can find N such that $A > A_k > A - \varepsilon$ holds for all the $k \geq N$ for any $\varepsilon > 0$. Hence

$$A > \sum_{i=1}^{m-2} \frac{1}{m} A_i = \frac{1}{m}\left(\sum_{i=1}^{N-1} A_i + \sum_{i=N}^{m-2} A_i\right) > \frac{m-N-1}{m}(A-\varepsilon).$$

Notice that

$$\lim_{m\to\infty} \frac{m-N-1}{m}(A-\varepsilon) = A - \varepsilon,$$

and thus have proven that for any $\varepsilon > 0$, $\lim_{m\to\infty} \sum_{i=1}^{m-2} \frac{1}{m} A_i > A - \varepsilon$.

Combined with the fact that $\sum_{i=1}^{m-2} \frac{1}{m} A_i < A$, we can conclude that

$$\lim_{m\to\infty} \sum_{i=1}^{m-2} \frac{1}{m} A_i = A = \lim_{n\to\infty} \frac{m-1}{m} A_{m-1}.$$

The proof is completed. □

Lemma 2 (Wielandt-Hoffman theorem [44]). *Given two Hermitian matrices A and B with eigenvalues α_k and β_k respectively, and α_k and β_k are ordered such that $\sum_k |\alpha_k - \beta_k|^2$ is minimized, then*

$$\frac{1}{m} \sum_{i=1}^{m} |\alpha_k - \beta_k|^2 \leq |A - B|^2.$$

We present the lemma for the purpose of self-completeness. Without loss of generality, we can assume that $\tau_{m,k}(\vec{r})$ and $\lambda_{m,k}(\vec{r})$ are in the same order, otherwise we could rotate the coordinate system to guarantee this property.

Lemma 3. *For any given integer s, we have*

$$\lim_{m\to\infty} \frac{1}{m} \sum_{k=1}^{m} \left(\tau^s_{m,k}(\vec{r}) - \lambda^s_{m,k}(\vec{r})\right) = 0.$$

Proof. Note that

$$\begin{aligned}
&\frac{1}{m} \sum_{k=0}^{m-1} \left|\tau^s_{m,k}(\vec{r}) - \lambda^s_{m,k}(\vec{r})\right| \\
&\frac{1}{m} \sum_{k=0}^{m-1} \left|\tau_{m,k}(\vec{r}) - \lambda_{m,k}(\vec{r})\right| \left|\sum_{k=0}^{m-1} \tau^k_{m,k}(\vec{r}) \lambda^{s-k-1}_{m,k}(\vec{r})\right| \\
&\leq \frac{s\Lambda^{s-1}}{n} \sum_{k=0}^{m-1} \left|\tau_{m,k}(\vec{r}) - \lambda_{m,k}(\vec{r})\right| \\
&\leq s\Lambda^{s-1} \sqrt{\frac{1}{m} \sum_{k=1}^{m} \left|\tau_{m,k}(\vec{r}) - \lambda_{m,k}(\vec{r})\right|^2} \\
&\leq s\Lambda^{s-1} |A - B|,
\end{aligned}$$

where Λ represents the upper bound of the eigenvalues, obviously s and Λ are constants with respect to m. The penult inequality is based on Cauchy-Schwarz Inequality and the last inequality is based on Lemma 2. Then the proof is completed. □

With Weierstrass' theorem, we know that there exists a sequence of polynomials $P_t(x)$ such that $\lim_{t\to\infty} P_t(x) = \frac{1}{x}$. For every fixed t, we know that $\lim_{m\to\infty} \frac{1}{m} \sum_{i=1}^{m} |P_t(\tau_{m,i}(\overrightarrow{r})) - P_t(\lambda_{m,i}(\overrightarrow{r}))| = 0$ according to Lemma 3. Hence combining the two equations above, we can obtain that

$$\lim_{m\to\infty} \frac{1}{m} \sum_{i=1}^{m} \left|\frac{1}{\tau_{m,i}} - \frac{1}{\lambda_{m,i}}\right| = 0.$$

Theorem 1. *The region $\mathbb{E}'$ is asymptotical equivalent to region $\mathbb{E}$:*

$$\begin{aligned}
&(1): \lim_{m\to\infty} \frac{1}{m} \Bigg\{ \sum_{i=1}^{m} \left[\frac{y_i{}^2}{\lambda_{m,i}(\vec{r})} - \frac{y_i{}^2}{\tau_{m,i}(\vec{r})}\right] - \sum_{i=1}^{m} \left[\frac{y_i{}^2}{\lambda_{m,i}(\vec{r'})} - \frac{y_i{}^2}{\tau_{m,i}(\vec{r'})}\right] \\
&\quad - \left[\frac{(y_1 + \sqrt{2}\delta\nabla\cos\theta)^2}{\lambda_{m,1}(\vec{r'})} - \frac{(y_1 + \sqrt{2}\delta\nabla\cos\theta)^2}{\tau_{m,1}(\vec{r'})}\right] \Bigg\} = 0; \\
&(2): \lim_{m\to\infty} \left\{ \ln \frac{|\Sigma(\vec{r})|^{\frac{1}{m}}}{|\Sigma(\vec{r'})|^{\frac{1}{m}}} - \ln \frac{|\Upsilon_m(\vec{r})|^{\frac{1}{m}}}{|\Upsilon_m(\vec{r'})|^{\frac{1}{m}}} \right\} = 0.
\end{aligned}$$

Proof. The RSS can be observed at each location is bounded, hence y_i^2s and $(y_1 + \sqrt{2}\delta\nabla\cos\theta)^2$ are bounded. Suppose that their upper bound is M, then

$$\begin{aligned}
&\frac{1}{m} \Bigg| \sum_{i=1}^{m} \left[\frac{y_i{}^2}{\lambda_{m,i}(\vec{r})} - \frac{y_i{}^2}{\tau_{m,i}(\vec{r})}\right] - \sum_{i=2}^{m} \left[\frac{y_i{}^2}{\lambda_{m,i}(\vec{r'})} - \frac{y_i{}^2}{\tau_{m,i}(\vec{r'})}\right] \\
&\quad - \left[\frac{(y_1 + \sqrt{2}\delta\nabla\cos\theta)^2}{\lambda_{m,1}(\vec{r'})} - \frac{(y_1 + \sqrt{2}\delta\nabla\cos\theta)^2}{\tau_{m,1}(\vec{r'})}\right] \Bigg| \\
&\leq \frac{2M}{m} \sum_{i=1}^{m} \left|\frac{1}{\tau_{m,k}(\vec{r})} - \frac{1}{\lambda_{m,k}(\vec{r})}\right|.
\end{aligned}$$

Combined with equation above Theorem 1, we know that the first part of theorem holds. The proof of the second part is similar. By using Weierstrass' theorem again, we know that there exists a sequence of polynomials $Q_t(\tau_{m,k}(\vec{r}))$ such that $\lim_{t\to\infty} P_t(\tau_{m,k}(\vec{r})) = \ln \tau_{m,k}(\vec{r})$. Combined with Lemma 3, we have

$$\lim_{m\to\infty} \frac{1}{m} \sum_{i=1}^{m} \left|\ln \tau_{m,k}(\vec{r}) - \ln \lambda_{m,k}(\vec{r})\right| = 0.$$

Notice that

$$\frac{1}{m} \sum_{i=1}^{m} \left|\ln \tau_{m,k}(\vec{r}) - \ln \lambda_{m,k}(\vec{r})\right| \geq \frac{1}{m} \left|\ln \frac{|\Sigma(\vec{r})|^{\frac{1}{m}}}{|\Upsilon_m(\vec{r})|^{\frac{1}{m}}}\right|,$$

which means that $\lim_{m\to\infty} \frac{1}{m} \left|\ln |\Sigma(\vec{r})|^{\frac{1}{m}} - \ln |\Upsilon_m(\vec{r})|^{\frac{1}{m}}\right| = 0$. With the same virtue, $\lim_{m\to\infty} \frac{1}{m} \left|\ln |\Sigma(\vec{r'})|^{\frac{1}{m}} - \ln |\Upsilon_m(\vec{r'})|^{\frac{1}{m}}\right| = 0$.

Combining these two equations, the second part of this theorem is proved. □

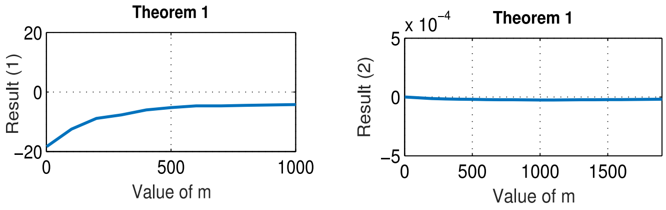

(a) Theorem 1 (1) (b) Theorem 1 (2)

Fig. 5. Convergence rate.

Fig. 5 provides the results of a brief numerical analysis of Equations (1) and (2) in Theorem 1. It can be seen that the two equations are being satisified as the value of m increases.

Theorem 2. *For any $\varepsilon > 0$, when $m > \max\{\frac{4N(\frac{\varepsilon\Delta^2}{4M})\frac{M}{\Delta^2}A}{\varepsilon}, \frac{N(\frac{\varepsilon\Delta}{2})}{\Delta\varepsilon}\}$, the difference of the expressions of these two regions is at most ε, where $N(\varepsilon)$ is the convergence rate of the series $\sum_{i=1}^{\infty}\rho_i^2$, that is, $\forall k > \varepsilon, \sum_{i=1}^{k}\rho_i^2 > A - \frac{\varepsilon}{2}$.*

Proof. Since $\sum_{i=1}^{\infty}\rho_i^2$ converges to A, then $\forall\varepsilon > 0$, there exists an integer $N(\varepsilon) > 0$, such that $\forall k > N(\varepsilon)$, $A \le A_k = \sum_{i=1}^{k}\rho_i^2 > A - \frac{\varepsilon}{2}$. Then we have

$$\sum_{i=1}^{m-1}\frac{i}{m}\rho_i^2(\vec{r}) = A_{m-1} - \sum_{i=1}^{m-1}\frac{A_i}{m} < A - \sum_{i=N(\varepsilon)}^{m-1}\frac{A_i}{m}$$
$$< A - (m - N(\varepsilon))\frac{A - \frac{\varepsilon}{2}}{m} = \frac{\varepsilon}{2} + \frac{N(\varepsilon)}{m}\left(A - \frac{\varepsilon}{2}\right).$$

And if $m > \frac{4N(\frac{\varepsilon\Delta^2}{4M})\frac{M}{\Delta^2}A}{\varepsilon}$, we have

$$\frac{1}{m}\left|\begin{array}{l}\sum_{i=1}^{m}\left[\frac{{y_i}^2}{\lambda_{m,i}(\vec{r})} - \frac{{y_i}^2}{\tau_{m,i}(\vec{r})}\right] - \sum_{i=2}^{m}\left[\frac{{y_i}^2}{\lambda_{m,i}(\vec{r'})} - \frac{{y_i}^2}{\tau_{m,i}(\vec{r'})}\right] \\ -\left[\frac{(y_1+\sqrt{2}\delta\nabla\cos\theta)^2}{\lambda_{m,1}(\vec{r'})} - \frac{(y_1+\sqrt{2}\delta\nabla\cos\theta)^2}{\tau_{m,1}(\vec{r'})}\right]\end{array}\right|$$
$$\le \frac{2M}{m}\sum_{i=1}^{m}\left|\frac{1}{\tau_{m,k}(\vec{r})} - \frac{1}{\lambda_{m,k}(\vec{r})}\right| \le \frac{2M}{\Delta^2}\sum_{i=1}^{m-1}\frac{i}{m}\rho_i^2(\vec{r})$$
$$< \frac{2M}{\Delta^2}\left(A - \left(m - N\left(\frac{\varepsilon\Delta^2}{4M}\right)\right)\frac{A - \frac{\varepsilon\Delta^2}{4M}}{m}\right)$$
$$= \frac{\varepsilon}{2} + \frac{N(\frac{\varepsilon\Delta^2}{4M})}{m}\left(\frac{2M}{\Delta^2}A - \frac{\varepsilon}{2}\right)$$
$$< \frac{\varepsilon}{2} + \frac{N(\frac{\varepsilon\Delta^2}{4M})}{\frac{4N(\frac{\varepsilon\Delta^2}{4M})\frac{M}{\Delta^2}A}{\varepsilon}}\left(\frac{2M}{\Delta^2}A - \frac{\varepsilon}{2}\right)$$
$$< \frac{\varepsilon}{2} + \frac{\varepsilon}{2} = \varepsilon.$$

Moreover, if $m > \frac{N(\frac{\varepsilon\Delta}{2})}{\Delta\varepsilon}$, we have

$$\frac{1}{m}\left|\ln\frac{|\Sigma(\vec{r})|^{\frac{1}{m}}}{|\Upsilon_m(\vec{r})|^{\frac{1}{m}}}\right| \le \frac{1}{m}\sum_{i=1}^{m}|\ln\tau_{m,k}(\vec{r}) - \ln\lambda_{m,k}(\vec{r})|$$
$$\le \frac{1}{\Delta}\sum_{i=1}^{m-1}\frac{i}{m}\rho_i^2(\vec{r}) \le \varepsilon.$$

Consequently, when $m > \max\left\{\frac{4N(\frac{\varepsilon\Delta^2}{4M})\frac{M}{\Delta^2}A}{\varepsilon}, \frac{N(\frac{\varepsilon\Delta}{2})}{\Delta\varepsilon}\right\}$, the difference of the expressions of these two regions is at most ε. $\square$

5.3 Boundaries of Region $\mathbb{E}'$

We define the *Fourier Transformation* of the covariance series as

$$g(\omega, \vec{r}) = \sum_{j=-\infty}^{\infty}\rho_j(\vec{r})e^{i2\pi\omega j}, -\frac{1}{2} < \omega \le \frac{1}{2}. \quad (18)$$

According to *Szego's theorem* [43], for an arbitrary continuous function G, we have

$$\lim_{m\to\infty}\frac{1}{m}\sum_{k=0}^{m-1}G(\tau_{m,k}(\vec{r})) = \int_{-1/2}^{1/2}G(g(\omega), \vec{r})d\omega. \quad (19)$$

Let $G(x) = \ln x$, we can obtain the approximate expression of the determinant of Σ_m

$$\ln|\Sigma_m(\vec{r})|^{1/m} = \frac{1}{m}\sum\ln\tau_{m,k}(\vec{r}) \approx \int_{-1/2}^{1/2}\ln g(\omega, \vec{r})d\omega. \quad (20)$$

For the matrix $\Sigma_m(\vec{r'})$, the corresponding Fourier Transformation is

$$\begin{aligned} g(\omega, \vec{r'}) &= \sum_{j=-\infty}^{\infty}\rho_j(\vec{r'})e^{i2\pi\omega j} \\ &= g(\omega, \vec{r}) + \delta\cos\theta\sum_{j=-\infty}^{\infty}|\nabla\rho_j(\vec{r})|e^{i2\pi\omega j}, \\ &-\frac{1}{2} < \omega \le \frac{1}{2}. \end{aligned} \quad (21)$$

Similarly, we can use

$$m\int_{-1/2}^{1/2}\ln[g(\omega, \vec{r}) + \delta\cos\theta\sum_{j=-\infty}^{\infty}|\nabla\rho_j(\vec{r})|e^{i2\pi\omega j}]d\omega, \quad (22)$$

to estimate the term $\ln|\Sigma_m(\vec{r'})|$.

Notice that

$$\begin{aligned} &\partial\frac{\ln\frac{|\Sigma_m(\vec{r})|^{\frac{1}{m}}}{|\Sigma_m(\vec{r'})|^{\frac{1}{m}}}}{\partial\theta} \\ &= \frac{\delta\sin\theta\sum_{j=-\infty}^{\infty}|\nabla\rho_j(\vec{r})|e^{i2\pi\omega j}}{g(\omega, \vec{r}) + \delta\cos\theta\sum_{j=-\infty}^{\infty}|\nabla\rho_j(\vec{r})|e^{i2\pi\omega j}} = O(\delta\sin\theta). \end{aligned} \quad (23)$$

Since δ is a bounded real number and $|\sin\theta| \le 1$,

$$\frac{d\ln\frac{|\Sigma_m(\vec{r})|^{\frac{1}{m}}}{|\Sigma_m(\vec{r'})|^{\frac{1}{m}}}}{d\theta} \approx 0. \quad (24)$$

Moreover, $\partial\frac{\left[\frac{(y_1+\sqrt{2}\delta\nabla\cos\theta)^2}{\lambda_i(\vec{r'})} + \sum_{i=1}^{m}\frac{{y_i}^2}{\lambda_i(\vec{r'})}\right]}{\partial\theta} = \sin\theta[h(\cos\theta) - c]$, where $h(\cdot)$ is a monotone function with respect to $\cos\theta$ and c is a positive number. Note that $\theta \in [0, \pi]$, thus there is at most one root of function $\sin\theta[h(\cos\theta) - c]$ in $[0, \pi]$. We use θ^* to denote this root; therefore, the minimum value of function $\frac{(y_1+\sqrt{2}\delta\nabla\cos\theta)^2}{\lambda_i(\vec{r'})} + \sum_{i=1}^{n}\frac{{y_i}^2}{\lambda_i(\vec{r'})}$ is achieved under these three cases: $\cos\theta = -1$, $\cos\theta = 1$ and $\cos\theta = \cos\theta^*$.

Consequently, the boundaries of the region $\mathbb{E}'$ can be described by the following three hypersurfaces:

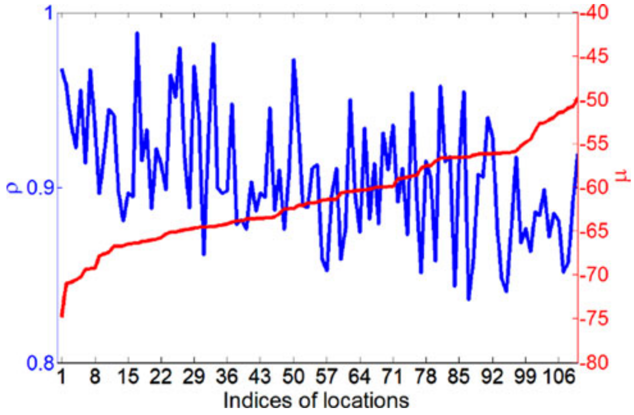

Fig. 6. Comparison of ρ and μ.

$$F_1 : \sum_{t=1}^{n} \frac{{y_i}^2}{\tau_{n,t}(\vec{r})} - \left[\frac{\left(y_1 - \sqrt{2}\delta\nabla\right)^2}{\tau_{n,1}(\vec{r}) - \delta\Delta\tau_{n,1}} + \sum_{t=2}^{n} \frac{{y_i}^2}{\tau_{n,t}(\vec{r}) - \delta\Delta\tau_{n,t}} \right] \leq \ln \frac{|\Sigma(\vec{r})|}{|\Sigma(\vec{r'})|}; \tag{25}$$

$$F_2 : \sum_{t=1}^{n} \frac{{y_i}^2}{\tau_{n,t}(\vec{r})} - \left[\frac{\left(y_1 + \sqrt{2}\delta\nabla\right)^2}{\tau_{n,1}(\vec{r}) + \delta\Delta\tau_{n,1}} + \sum_{t=2}^{n} \frac{{y_i}^2}{\tau_{n,t}(\vec{r}) + \delta\Delta\tau_{n,t}} \right] \leq \ln \frac{|\Sigma(\vec{r})|}{|\Sigma(\vec{r'})|}; \tag{26}$$

$$F_3 : \sum_{t=1}^{n} \frac{{y_i}^2}{\tau_{n,t}(\vec{r})} - \left[\frac{\left(y_1 + \sqrt{2}\delta\cos\theta^*\nabla\right)^2}{\tau_{n,1}(\vec{r}) + \delta\cos\theta^*\Delta\tau_{n,1}} + \sum_{t=2}^{n} \frac{{y_i}^2}{\tau_{n,t}(\vec{r}) + \delta\cos\theta^*\Delta\tau_{n,t}} \right] \leq \ln \frac{|\Sigma(\vec{r})|}{|\Sigma(\vec{r'})|}. \tag{27}$$

6 Location Estimation Facilitated by Temporal Correlation

6.1 Feasibility of Utilizing Temporal Correlation

We first investigate whether location estimation could be facilitated with the information of temporal correlation in practice. We conduct experiments in a square indoor space that is a around $40\ m^2$. The square is divided into grids with the edge length of 60 cm. Fig. 6 associates the values of μ and ρ with locations, where the horizontal axis represents the indices of locations. We sort the locations according to the locally sampled values of μ, and the corresponding values of ρ are also plotted. It can be seen that the values of ρ present distinct pattern compared with μ in each location. In fact, we calculate the cross correlation between μ and ρ, and the results indicate that the two values are not related to each other. The experiment results illustrated above indicate that the temporal correlation information of the RSS provides a diversified feature compared with the information of μ. The temporal correlation could be used to cross check the result of location estimation. It is worth mentioning that the values of ρ can be derived from the sampled RSSes thus incur no extra overhead in the training phase. The spatial distribution of μ and ρ are illustrated and analyzed, which could be found in our technical report [15].

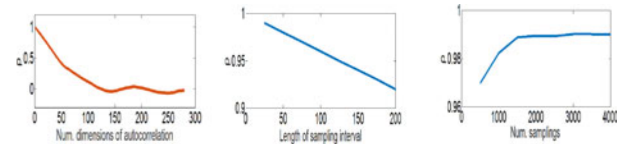

(a) Number of correlation dimensions (b) Sampling interval (c) Number of samplings

Fig. 7. Experiments for choice of design parameters.

6.2 Localization Estimation Algorithm

The basic idea of the algorithm is that we first find a list of candidate locations of the user with the mean value comparison as most of the work in the literature does, and then find the most likely location with the temporal correlation comparison. Algorithm 1 illustrates how to utilize temporal correlation for better location estimation, which is in essence a synthetic approach integrating the information of both the mean value and the temporal correlation of the RSS. Detailed methods for finding parameters μ and ρ could be found in our technical report [15].

Algorithm 1. Temporal Correlation for Location Estimation

Input parameters:
The training data set for each location $\vec{r}$, x_{ij} $(i = 1\dots n;\ j = 1\dots w)$;
The reported RSS sequence t_{ij} $(i = 1\dots a;\ j = 1\dots b)$ from a user;
Indoor space L is a set of all the identified locations recorded in the database;
Threshold Th is the critical value of choice for mean vectors.

1) For each location i in L, calculate the mean vector $\mu_{\mathbf{i}} = (\mu_1, \mu_2, \dots, \mu_m)$, and the correlation vector $\rho_{\mathbf{i}} = (\rho_1, \rho_2, \dots, \rho_m)$.
2) For the reported data t_{ij} from a user, also calculate the target mean and correlation vectors as μ_t, ρ_t.
3) Find the Euclidean distance between $\mu_{\mathbf{t}}$ and every $\mu_{\mathbf{i}}$. Find all the vectors $\mu_{\mathbf{k}}$ among those $\mu_{\mathbf{i}}$s, and the distance between each $\mu_{\mathbf{k}}$ and $\mu_{\mathbf{t}}$ should be within Th in the sample space, i.e., $|\mu_{\mathbf{i}} - \mu_{\mathbf{t}})| <= Th$. The corresponding locations associated with those $\mu_{\mathbf{k}}$s are denoted using a set $\{\mathbf{l_{kmin}}\}$.
4) Compare the Euclidean distance between ρ_t and ρ_i in $\{\mathbf{l_{kmin}}\}$. Find the vector that is nearest to ρ_t. The nearest distance in correlation sample space is the place we localize the user at.

6.3 Choice of Design Parameters

Design parameters must be chosen before the algorithm presented above can be appropriately utilized. We conduct experiments to show how parameters such as the number of temporal dimension, the sampling interval and number of samplings could influence the value of ρ in a location. A distinguishable value of ρ in a location is favored in the localization process.

We calculate the temporal correlation coefficient ρ from 2-dimension to 280-dimension. The results are shown in Fig. 7a. We can find that the value of ρ decreases as the number of dimensions increases and then keeps

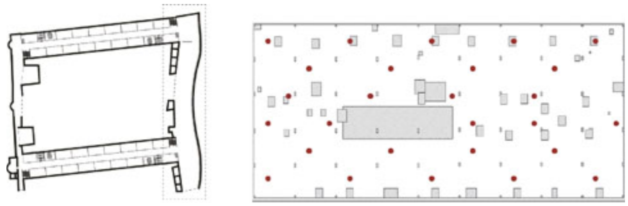

(a) Local experiment field.

(b) Room Zwijnaarde of EVARILOS testbed [48].

Fig. 8. Floor plans of test fields.

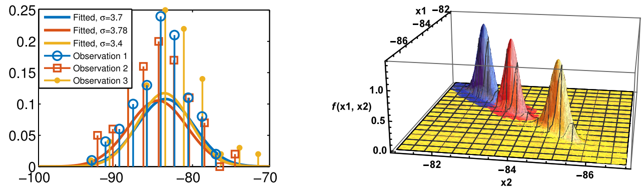

(a) Gaussian Distribution

(b) Gaussian Process

Fig. 9. Modeling approach.

comparatively flat. The value of ρ is at around 0 when the number of dimensions goes beyond 100, which indicates that it is meaningless to consider over-high dimensions. The current value of RSS becomes almost irrelevant compared with the values of RSS sampled long time ago. We can also find that the number of dimensions 50 is a critical point, after which the trend of ρ becomes flat. Consequently, we recommend to utilize the information the temporal correlation with the number of dimensions less then 50 in practice.

The effectiveness of the temporal correlation also depends on the length of the interval that sequential RSS samplings are performed. Fig. 7b shows the corresponding values of ρ under different sampling intervals varying from 25 to $200\ \mathrm{ms}$. It is straightforward that the values of ρ are decreasing as the length of the interval increases, because the longer the interval is the more unrelated the currently sampled RSS value is from the previous ones. However, over-short sampling interval is also unnecessary, since the RSS readings may not change that fast and the observed values of the RSS are basically the same in this case. We choose $100\ \mathrm{ms}$ as the length of sampling interval, which is proved to be appropriate in the experiments to be presented later.

After the number of dimensions and the sampling interval are determined, we still need to decide the starting point of the sampling in practice. This is because we could see variance of ρ at the first amount of sampling intervals, as shown in Fig. 7c. We need to retrieve those RSSes that yields comparatively stable temporal correlation information. To this end, we sample 2,000 RSS values in our system, since the value of ρ tends to be stable after the 1,500th sampling as shown in the sub-figure.

7 Experimental Results

We conduct local experiments and use trace data experiments to verify our model and show the performance of the proposed localization algorithm, where the floor plans are shown as in Fig. 8. Detailed descriptions of EVARILOS testbed and the Zwijnaarde room could be found in [45], [46], [47], [48]. We first provide experimental results to verify our modeling assumption, and then show the influence of the temporal correlation property on the reliability and accuracy of location estimation.

Verification of the Modeling Assumption. We did local experiments to verify the modeling assumption in the conference version [14]. We here use the trace data from EVARILOS testbed to further verify the Gaussian assumption. We first filter out those unreliable measurements in the trace data, where there is only 1 or 2 RSS readings recorded or all the RSS readings are exactly the same. We observe the RSS values in three locations (1,290, 1,980), (1,290, 1,270) and (1,890, 1,270), which are with respect to the AP located at (1,000, 1,712). We calculate the probability each value appears and find that they are approximately to be Gaussian distribution as shown in Fig. 9a, with skewness and kurtosis less than $|0.5|$ and $|3.3|$ respectively. The resulted joint PDFs are as shown in Fig. 9b. The experimental results support our modeling assumption that the signal could be modeled following Gaussian distribution.

Influence on Localization Reliability. We conduct local experiments to examine whether the temporal correlation information of the RSS could improve the reliability of fingerprinting based localization in practice. We choose to use local experiments because the distance among reference points in the experiment can be controlled freely, which is important to examine the reliability improvement when the error tolerance metric is very small. In particular, we use the value of μ and ρ with respect to different APs at each location as the local fingerprints in the localization database. At each sampling location, we collect totally 4,000 RSS fingerprints at the sampling interval of $25\ \mathrm{ms}$ with respect to each Wi-Fi AP available. In the localization phase, we sample totally 1,500 fingerprints at the sampling interval of $25\ \mathrm{ms}$, where the top 5 strongest fingerprints are sampled. We compare the mean value of the sampled fingerprints and those have been stored in the database with the K-nearest neighbors (KNN) algorithm [3]. In particular, we find sampled RSSes' neighbors that are within a threshold Th in the sample space, and put the corresponding associated locations on a list. For each location on the list, we examine the corresponding values of ρ with that of the sampled RSSes. The location with the most matched ρ will be determined as the estimated location of the user.

We evaluate the localization performance by considering both the accuracy and reliability. In the experiment, we first set the error tolerance radius δ, which means that any estimated locations within the δ neighborhood of the user's actual location can be regarded as a correct estimation. We set different radius and randomly pick up 500 estimations to evaluate the performance. With the results of localization, we could find the probability that the user's location is correctly estimated, which is termed as reliability.

The experiment results are illustrated in Fig. 10. The radius is set to be 30, 60, 120 and $180\ \mathrm{cm}$, respectively. In each case, we increase the threshold Th from 0 to 5. Note that the unit of the threshold is not important, as we consider the normalized distance in the sample space. As shown in Fig. 10, the localization reliability increases first and then decreases as the threshold increases in all scenarios.

If the threshold is 0, the user's location is basically estimated using the mean of the RSSes; the information of the temporal correlation is not utilized. If the threshold increases, the system could cross check the candidate locations and find

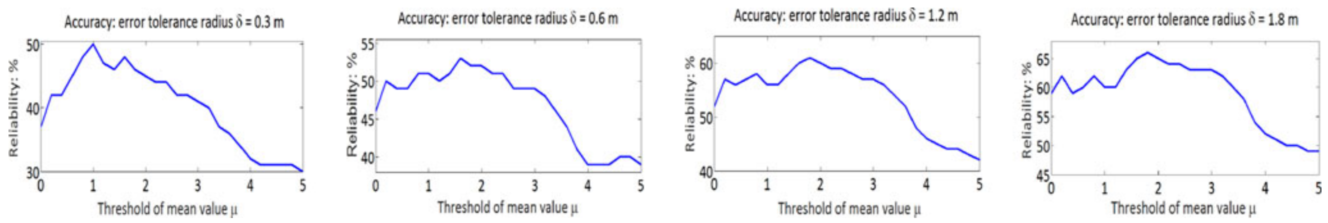

Fig. 10. Reliability with different threshold Th and error tolerance radius.

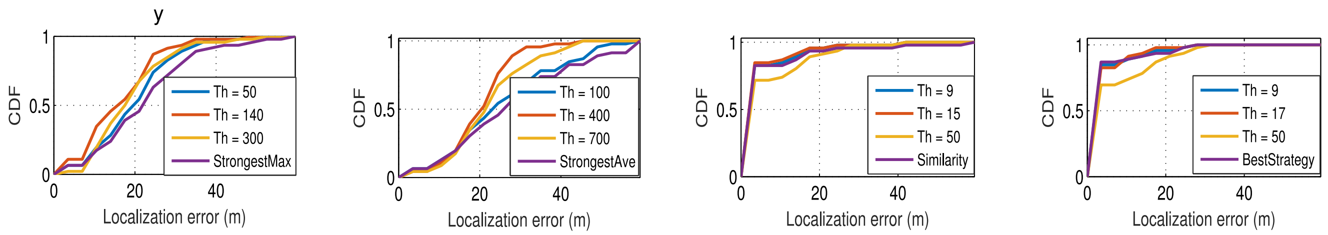

Fig. 11. CDF of localization errors with different AP selection schemes.

the most matched one; therefore, the reliability is improved. If the threshold is large enough, it means that more candidate locations could be on the list. Since those locations are picked up according to their corresponding fingerprints in the sample space, they may be far away from each other in the physical space. The observed temporal correlation information is unable to effectively tell one location from another. The more the candidate locations are, the higher probability that the location is far from the APs, and the temporal correlation becomes indistinguishable. That is why the reliability becomes worse if the threshold is too large. More detailed experiments data can be found in our technical report [15]. It is shown that the reliability of the fingerprinting localization could be improved by up to 13 percent if we choose the radius of 0.3 m and the threshold of 1.

Influence on Localization Accuracy. With the trace data, we use the location estimation scheme as shown in Algorithm 1

TABLE 1
Experimental Results with EVARILOS Trace Data

$Metric[m]$	$StrgstMax$	$Th = 50$	$Th = 140$	$Th = 300$
Avg.err	19.0	16.1	12.8	15.0
Min.err	4.0	3.8	3.6	3.5
Max.err	53.9	43.4	43.4	45.7
Med.err	19.0	15.7	12.2	14.0
$Metric[m]$	$StrgstAvg$	$Th = 100$	$Th = 400$	$Th = 700$
Avg.err	24.1	21.9	16.3	18.6
Min.err	3.8	4.0	3.8	3.5
Max.err	55.0	54.0	40.2	40.2
Med.err	22.5	18.9	16.2	18.0
$Metric[m]$	$Similarity$	$Th = 9$	$Th = 15$	$Th = 50$
Avg.err	7.1	6.0	5.7	7.8
Min.err	3.5	3.8	3.6	3.5
Max.err	54.0	41.1	41.1	41.1
Med.err	3.5	3.8	3.6	3.5
$Metric[m]$	$BestStrategy$	$Th = 9$	$Th = 17$	$Th = 50$
Avg.err	6.4	6.4	5.8	9.5
Min.err	4.0	3.8	3.5	3.6
Max.err	28.1	28.1	28.1	31.5
Med.err	4.0	4.0	3.5	3.5

and the regular mean comparison algorithm to perform localization respectively, in order to evaluate the influence of temporal correlation information usage on the localization accuracy. We compare the two location estimation schemes under different AP selection schemes. With *StrongestAvg*, the user measures APs with the strongest average RSSes can be observed at the to-be-determined location in the online phase. With *StrongestMax*, the user measures APs with the strongest RSSes can be observed. With the *Similarity* strategy, APs are first clustered according to the similarity of their generated RSSes and the representative AP of each cluster is then selected. How to compute the similarity metric and how to select the representative AP in a cluster are described in [12]. The algorithm for the *BestStrategy* is shown in [13], [16]

After APs are selected, we could run algorithms for localization with and without taking temporal correlation into account. The experiment results are shown in Fig. 11 and detailed statistical results are tabulated in Table 1. In Fig. 11a, the curve labeled with "StrongestMax" means the results obtained with mean comparison and the APs used in the online phase are selected with the StrongestMax method; the curves labeled with different values of the threshold Th represent the results obtained with the proposed location estimation algorithm. The meanings of curves in other 3 sub-figures could be understood by the analogy. It can be seen from Table 1 that the overall performance of the localization mechanism considering temporal correlation of the RSS is better than the regular mechanism under different AP selection schemes, where choosing appropriate value of the threshold is vitally important. In particular, when choosing appropriate threshold, the maximum average error reduction is around 30 percent. It is worth noting that the accuracy improvement is less significant if the more advanced AP selection scheme is used, this is because the room for accuracy improvement is reduced under such schemes.

8 Conclusion and Future Work

In this paper, we have theoretically shown that the temporal correlation of the RSS can further improve accuracy of the fingerprinting localization. In particular, we have constructed a theoretical framework to evaluate how the temporal correlation of the RSS can influence reliability of location estimation, which is based on a newly proposed radio propagation model considering the time-varying property of signals from Wi-Fi APs. The framework has been applied to analyze localization in the one dimensional physical space, which reveals the fundamental reason why localization performance can be improvement by leveraging temporal correlation of the RSS. We have extended our analysis to high-dimensional scenarios and mathematically depict the boundaries in the RSS sample space, which distinguish one physical location from another. Moreover, we have developed an algorithm to utilize temporal correlation of the RSS to improve the location estimation accuracy, where the process for choosing key design parameters are provided through experiments. Experiment results show that the localization reliability and accuracy can be improved by up to 13 and 30 percent with appropriate leveraging the RSS temporal correlation. Our future work will investigate how the threshold in Algorithm 1 should be set appropriately, and the influence of body-shadowing on the capacity of the fingerprinting based localization system.

ACKNOWLEDGMENTS

This work is supported by the National Natural Science Foundation of China (No. 61572319, U1405251, 61532012, 61428205, 61325012, 61271219, 61428205). A preliminary version of this article appears in the *Proceedings of the 35th IEEE International Conference on Computer Communications* (IEEE INFOCOM 2016).

REFERENCES

[1] Z. Yang, Z. Zhou and Y. Liu, "From RSSI to CSI: Indoor localization via channel response," *ACM Comput. Surveys*, vol. 46, no. 2, pp. 1–32, 2013.

[2] H. Liu, et al., "Push the limit of WiFi based localization for smartphones," in *Proc. 18th Annu. Int. Conf. Mobile Comput. Netw.*, 2012, pp. 305–316.

[3] H. Liu, J. Yang, S. Sidhom, Y. Wang, Y. Chen, and F. Ye, "Accurate WiFi based localization for smartphones using peer assistance," *IEEE Trans. Mobile Comput.*, vol. 13, no. 10, pp. 2199–2214, Oct. 2013.

[4] A. Rai, K. K. Chintalapudi, V. N. Padmanabhan, and R. Sen, "Zee: Zero-effort crowdsourcing for indoor localization," in *Proc. 18th Annu. Int. Conf. Mobile Comput. Netw.*, 2012, pp. 293–304.

[5] S. Fang, B. Lu, and Y. Hsu, "Learning location from sequential signal strength based on GSM experimental data," *IEEE Trans. Veh. Technol.*, vol. 61, no. 2, pp. 726–736, Feb. 2012.

[6] S. Fang and T. Lin, "A dynamic system approach for radio location fingerprinting in wireless local area networks," *IEEE Trans. Commun.*, vol. 58, no. 4, pp. 1020–1025, Apr. 2010.

[7] S. Kuo and Y. Tseng, "A scrambling method for fingerprint positioning based on temporal diversity and spatial dependency," *IEEE Trans. Knowl. Data Eng.*, vol. 20, no. 5, pp. 678–684, May 2008.

[8] G. Chandrasekaran, et al., "Empirical evaluation of the limits on localization using signal strength," in *Proc. 6th Annu. IEEE Commun. Soc. Conf. Sensor Mesh Ad Hoc Commun. Netw.*, 2009, pp. 1–9.

[9] N. Patwari, J. Ash, S. Kyperountas, A. O. Hero, R. Moses, and N. Correal, "Locating the nodes: Cooperative localization in wireless sensor networks," *IEEE Signal Process. Mag.*, vol. 22, no. 4, pp. 55–69, Jul. 2005.

[10] N. Patwari, A. O. H. III, M. Perkins, N. S. Correal, and R. J. O'Dea, "Relative location estimation in wireless sensor networks, *IEEE Trans. Signal Process.*, vol. 51, no. 8, pp. 2137–2148, Aug. 2003.

[11] M. Angjelichinoski, D. Denkovski, V. Atanasovski, and L. Gavrilovska, "Cramér-Rao lower bounds of RSS-based localization with anchor position uncertainty," *IEEE Trans. Inf. Theory*, vol. 61, no. 5, pp. 2807–2834, May 2015.

[12] K. Chintalapudi, A. Padmanabha Iyer, and V. N. Padmanabhan, "Indoor localization without the pain," in *Proc. Annu. Int. Conf. Mobile Comput. Netw.*, 2010, pp. 173–184.

[13] Y. Wen, X. Tian, X. Wang, and S. Lu, "Fundamental limits of RSS fingerprinting based indoor localization," in *Proc. IEEE Conf. Comput. Commun.*, 2015, pp. 2479–2487.

[14] M. Wang, Z. Zhang, X. Tian, and X. Wang, "Temporal correlation of the RSS improves accuracy of fingerprinting localization," in *Proc. 35th Annu. IEEE Conf. Comput. Commun.*, 2016, pp. 1–9.

[15] Technical report, 2016. [Online]. Available: https://www.dropbox.com/s/0jxjf5nalrnz8vn/IEEE%20TMC-Temporal-Technical%20report.pdf?dl=0

[16] Z. Zhang, D. Liu, S. Zhu, S. Chen, and X. Tian, "Squeeze more from fingerprints reporting strategy for indoor localization," in *Proc. 13th Annu. IEEE Commun. Soc. Conf. Sensor Mesh Ad Hoc Commun. Netw.* 2016, pp. 1–9.

[17] K. Kaemarungsi and P. Krishnamurthy, "Modeling of indoor positioning systems based on location fingerprinting," in *Proc. IEEE INFOCOM*, 2004, pp. 400–408.

[18] M. Youssef and A. Agrawala, "The Horus WLAN location determination system," in *Proc. 3rd Int. Conf. Mobile Syst. Appl. Services*, 2005, pp. 205–218.

[19] H. Hashemi, "Impulse response modeling of indoor radio propagation channels," *IEEE J. Sel. Areas Commun.*, vol. 11, no. 7, pp. 967–978, Sep. 2006.

[20] M. Youssef and A. Agrawala, "Handling samples correlation in the Horus system," in *Proc. IEEE INFOCOM*, 2004, pp. 1023–1031.

[21] M. Youssef, M. Abdallah, and A. Agrawala, "Multivariate analysis for probabilistic WLAN location determination systems," in *Proc. 2nd Annu. Int. Conf. Mobile Ubiquitous Syst.: Netw. Services*, 2005, pp. 353–362.

[22] C. Oestges, N. Czink, B. Bandemer, P. Castiglione, F. Kaltenberger, and J. Paulraj, "Experimental characterization and modeling of outdoor-to-indoor and indoor-to-indoor distributed channels," *IEEE Trans. Veh. Technol.*, vol. 59, no. 5, pp. 2253–2265, Nov. 2010

[23] C. Fischione, F. Graziosi, and F. Santucci, "Approximation for a sum of on-off lognormal processes with wireless applications," *IEEE Trans. Commun.*, vol. 55, no. 10, pp. 1984–1993, Oct. 2007.

[24] F. Graziosi and F. Santucci, "A general correlation model for shadow fading in mobile radio systems," *IEEE Commun. Lett.*, vol. 6, no. 3, pp. 102–104, Mar. 2002

[25] C. Oestges, N. Czink, B. Bandemer, P. Castiglione, F. Kaltenberger, and J. Paulraj, "Experimental characterization and modeling of outdoor-to-indoor and indoor-to-indoor distributed channels," *IEEE Trans. Veh. Technol.*, vol. 59, no. 5, pp. 2253–2265, Nov. 2010.

[26] F. Graziosi and F. Santucci, "A general correlation model for shadow fading in mobile radio systems," *IEEE Commun. Lett.*, vol. 6, no. 3, pp. 102–104, Mar. 2002

[27] S. Obayashi and J. Zander, "A body-shadowing model for indoor radio communication environments view document," *IEEE Trans. Antennas Propag.*, vol. 46, no. 6, pp. 920–927, Jun. 1998.

[28] M. Ayadi and A. Zineb, "Body shadowing and furniture effects for accuracy improvement of indoor wave propagation models," *IEEE Trans. Wireless Commun.*, vol. 13, no. 11, pp. 5999–6006, Nov. 2014

[29] I. Kashiwagi, T. Taga, and T. Imai, "Time-varying path-shadowing model for indoor populated environments view document," *IEEE Trans. Veh. Technol.*, vol. 59, no. 1, pp. 16–28, Jan. 2010.

[30] S. Szyszkowicz, H. Yanikomeroglu, and J. Thompson, "On the feasibility of wireless shadowing correlation models," *IEEE Trans. Veh. Technol.*, vol. 59, no. 9, pp. 4222–4236, Nov. 2010.

[31] D. Vasisht, S. Kumar, and D. Katabi, "Decimeter-Level location with a single WiFi access point," in *Proc. 13th Usenix Conf. Netw. Syst. Des. Implementation*, Mar. 2016, pp. 165–178.

[32] M. Kotaru, K. Joshi, D. Bharadia, and S. Katti, "SpotFi: Decimeter level localization using WiFi," in *Proc. ACM Conf. Special Interest Group Data Commun.*, Aug. 2015, pp. 269–282.

[33] S. Kumar, S. Gil, D. Katabi, and D. Rus, "Accurate indoor localization with zero start-up cost," in *Proc. 20th Annu. Int. Conf. Mobile Comput. Netw.*, Sep. 2014, pp. 483–494.

[34] D. Halperin, W. Hu, A. Sheth, and D. Wetherall, "Tool release: Gathering 802.11n traces with channel state information," *ACM SIGCOMM Comput. Commun. Rev.*, vol. 41, pp. 53–53, Jan. 2011.

[35] K. Kaemarungsi and P. Krishnamurthy, "Properties of indoor received signal strength for WLAN location fingerprinting," in *Proc. 1st Annu. Int. Conf. Mobile Ubiquitous Syst.: Netw. and Services*, Aug. 2004, pp. 14–23.

[36] K. Kaemarungsi and P. Krishnamurthy, "Modeling of indoor positioning systems based on location fingerprinting," in *Proc. IEEE INFOCOM*, Mar. 2004, pp. 1012–1022.
[37] E. Elnahrawy, X. Li, and R. P. Martin, "The limits of localization using signal strength: A comparative study," in *Proc. 1st Annu. IEEE Commun. Soc. Conf. Sensor Ad Hoc Commun. Netw.*, 2004, pp. 406–414.
[38] K. Chintalapudi, A. Padmanabha Iyer, and V. N. Padmanabhan, "Indoor localization without the pain," in *Proc. 16th Annu. Int. Conf. Mobile Comput. Netw.*, 2010, pp. 173–184.
[39] M. Win, et al., "Network localization and navigation via cooperation," *IEEE Commun. Mag.*, vol. 49, no. 5, pp. 56–62, May 2011.
[40] W. Dai, Y. Shen, and M. Win, "Energy-efficient network navigation algorithms," *IEEE J. Sel. Areas Commun.*, vol. 33, no. 7, pp. 1418–1430, Jul. 2011.
[41] H. Wymeersch, J. Lien, and M. Win, "Cooperative localization in wireless network," *Proc. IEEE*, vol. 97, no. 2 pp. 427–450, Feb. 2009.
[42] T. Wang, Y. Shen, S Mazuelas, H. Shin, and M. Win, "On OFDM ranging accuracy in multipath channels," *IEEE Syst. J.*, vol. 8, no. 1, pp. 104–114, Mar. 2014.
[43] U. Grenander and G. Szegö, *Toeplitz forms and Their Applications*, vol. 321. Berkeley, CA, USA: Univ. of California Press, 2001.
[44] L. D. Branges, "The Stone-Weierstrass theorem," *Proc. Amer. Math. Soc.*, vol. 5, no. 4, pp. 822–824, 1959.
[45] EVARILOS testbed. (2016). [Online]. Available: http://evarilos.intec.ugent.be/
[46] T. V. Haute, et al., "Platform for benchmarking of RF-based indoor localization solutions," *IEEE Commun. Mag.*, vol. 53, no. 9, pp. 126–133, Sep. 2015.
[47] T. V. Haute, et al., "Comparability of RF-based indoor localization solutions in heterogeneous environments: An experimental study," *Int. J. Ad Hoc Ubiquitous Comput.*, vol. 23, no. 1/2, pp. 92–114, 2016.
[48] F. Lemic, A. Behboodi, V. Handziski, and V. Wolisz, "Experimental decomposition of the performance of fingerprinting-based localization algorithms," in *Proc. Int. Conf. Indoor Positioning Indoor Navigat.* 2016, pp. 695–704.

Xiaohua Tian (S'07-M'11) received the BE and ME degrees in communication engineering from Northwestern Polytechnical University, Xian, China, in 2003 and 2006, respectively, and the PhD degree from the Department of Electrical and Computer Engineering (ECE), Illinois Institute of Technology (IIT), Chicago, in Dec. 2010. Since Mar. 2011, he has been in the School of Electronic Information and Electrical Engineering, Shanghai Jiao Tong University, and now is an associate professor with the title of SMC-B scholar. He serves as the column editor of the *IEEE Network Magazine* and the guest editor of the *International Journal of Sensor Networks* (2012). He also serves/served as the TPC member for IEEE INFOCOM 2014-2017, best demo/poster award committee member of IEEE INFOCOM 2014, TPC co-chair for IEEE ICCC 2014-2016, TPC Co-chair for the 9th International Conference on Wireless Algorithms, Systems and Applications (WASA 2014), TPC member for IEEE GLOBECOM 2011-2016, and TPC member for IEEE ICC 2013-2016, respectively. He is a member of the IEEE.

Mei Wang received the BE degree in information engineering from Shanghai Jiao Tong University, in 2016. Her main areas of research are mobile computing, signal processing, and wireless network.

Wenxin Li received the BS (with Hons.) degree in automation from Shanghai Jiao Tong University, in 2016. His research interests include scheduling algorithm design, coded caching, and indoor localization.

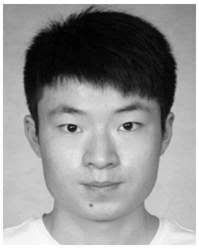

Binyao Jiang is currently working toward the BE degree in computer science from Shanghai Jiao Tong University, China, and is expected to graduate in 2019. His recent research work is on indoor localization.

Dong Xu is currently working toward the BE degree in electronics engineering from Shanghai Jiao Tong University, China, and is expected to graduate in 2017. His recent research work is on indoor localization.

Xinbing Wang received the BS (with Hons.) degree from the Department of Automation, Shanghai Jiaotong University, Shanghai, China, in 1998, the MS degree from the Department of Computer Science and Technology, Tsinghua University, Beijing, China, in 2001, and the PhD degree, major from the Department of electrical and Computer Engineering, minor from the Department of Mathematics, North Carolina State University, Raleigh, in 2006. Currently, he is a professor in the Department of Electronic Engineering, Shanghai Jiaotong University, Shanghai, China. He has been an associate editor of the *IEEE/ACM Transactions on Networking* and the *IEEE Transactions on Mobile Computing*, and a member of the technical program committees of several conferences including ACM MobiCom 2012, ACM MobiHoc 2012-2014, and IEEE INFOCOM 2009-2017. He is a senior member of the IEEE.

Jun Xu is a professor in the School of Computer Science, Georgia Institute of Technology. A major thrust of his research lies in network algorithmics, the science of designing high-speed Internet routers, firewalls, and measurement devices. He received ACM Sigmetrics 2004 Best Student Paper Award, and has been an ACM Distinguished Scientist since 2010.